

UNIVERSIDAD SAN FRANCISCO DE QUITO USFQ

Colegio de Ciencias e Ingenierías

In silico study of the racemization mechanism of aliphatic and aromatic amino acids

Mateo Santiago Andino León

Ingeniería Química

Trabajo de fin de carrera presentado como requisito
para la obtención del título de
Ingeniero Químico

Quito, 02 de mayo de 2023

UNIVERSIDAD SAN FRANCISCO DE QUITO USFQ

Colegio de Ciencias e Ingenierías

HOJA DE CALIFICACIÓN DE TRABAJO DE FIN DE CARRERA

**In silico study of the racemization mechanism of aliphatic and
aromatic amino acids**

Mateo Santiago Andino León

Nombre del profesor, Título académico

José Mora, Ph. D.

Nombre del profesor, Título académico

Juan Diego Fonseca, Ph. D.

Quito, 02 de mayo de 2023

© DERECHOS DE AUTOR

Por medio del presente documento certifico que he leído todas las Políticas y Manuales de la Universidad San Francisco de Quito USFQ, incluyendo la Política de Propiedad Intelectual USFQ, y estoy de acuerdo con su contenido, por lo que los derechos de propiedad intelectual del presente trabajo quedan sujetos a lo dispuesto en esas Políticas.

Asimismo, autorizo a la USFQ para que realice la digitalización y publicación de este trabajo en el repositorio virtual, de conformidad a lo dispuesto en la Ley Orgánica de Educación Superior del Ecuador.

Nombres y apellidos: Mateo Santiago Andino León

Código: 00205230

Cédula de identidad: 1721536843

Lugar y fecha: Quito, 02 de mayo de 2023

ACLARACIÓN PARA PUBLICACIÓN

Nota: El presente trabajo, en su totalidad o cualquiera de sus partes, no debe ser considerado como una publicación, incluso a pesar de estar disponible sin restricciones a través de un repositorio institucional. Esta declaración se alinea con las prácticas y recomendaciones presentadas por el Committee on Publication Ethics COPE descritas por Barbour et al. (2017) Discussion document on best practice for issues around theses publishing, disponible en <http://bit.ly/COPETHeses>.

UNPUBLISHED DOCUMENT

Note: The following capstone project is available through Universidad San Francisco de Quito USFQ institutional repository. Nonetheless, this project – in whole or in part – should not be considered a publication. This statement follows the recommendations presented by the Committee on Publication Ethics COPE described by Barbour et al. (2017) Discussion document on best practice for issues around theses publishing available on <http://bit.ly/COPETHeses>.

RESUMEN

La racemización de biomoléculas es la principal causa de la pérdida de actividad óptica en fármacos. La dependencia de equipos costosos para caracterizar enantiómeros en reacciones de racemización hace que el diseño experimental sea desafiante, así como la dependencia del producto en diferentes condiciones de reacción. Los aminoácidos aromáticos han demostrado disminuir la energía de activación de racemización en comparación a los aminoácidos alifáticos, y sustituyentes aromáticos desactivantes proporciona la mayor estabilización de los estados de transición. El efecto de la aromaticidad en la racemización se estudia teóricamente mediante cálculos de teoría del funcional de densidad a nivel $\omega b97xd/6-311++g(d,p)$. Se propone un intermediario carbaniónico para explicar la estabilización aromática observada a través de resonancia. El análisis de Hammett confirmó la formación de carga negativa en el estado de transición de los compuestos aromáticos, y cálculos de orbitales naturales de enlace (NBO) junto con coordenadas de reacción intrínsecas (IRC) confirmaron la estabilización de la distribución electrónica hacia el intermediario carbaniónico. Sin embargo, el análisis IRC de energía mostró que los aminoácidos alifáticos requieren un mayor trabajo de reacción en la reorganización estructural para alcanzar un intermediario energéticamente igual al estado de transición, lo que implica que estos compuestos podrían seguir un mecanismo de reacción diferente.

Palabras clave: Racemización, aminoácidos, teoría del funcional de densidad, coordenadas de reacción intrínsecas, orbitales naturales de enlace.

ABSTRACT

Racemization of biomolecules is the main cause of the loss of optical activity of pharmaceutical drugs. The reliance on expensive equipment to characterize enantiomers in racemization reactions makes experimental design challenging, as well as the product dependence on different reaction conditions. Aromatic amino acids imply a lower activation energy for racemization when compared to aliphatic amino acids, and when using deactivating aromatic substituents, a bigger stabilization of the transition states is obtained. The effect of aromaticity in racemization is studied theoretically through density functional theory calculations at the $\omega b97xd/6-311++g(d,p)$ level of theory. A carbanion intermediate is proposed to explain the observed aromatic stabilization through resonance. Hammett analysis confirmed the formation of a negative charge towards the transition state of aromatics, and natural bond orbital (NBO) coupled with intrinsic reaction coordinates (IRC) calculations confirmed the stabilization of electron distribution towards the carbanion intermediate. Nevertheless, energy IRC showed that aliphatic amino acids require greater reaction work in structural rearrangement to reach an intermediate energetically similar to the transition state, thus implying that these compounds could follow a different reaction mechanism.

Keywords: Racemization, amino acids, density functional theory, intrinsic reaction coordinates, natural bond orbital.

TABLA DE CONTENIDO

Resumen	5
Abstract.....	6
Tabla de contenido	7
Índice de tablas	8
Índice de figuras	9
1. Introduction.....	11
2. Methodology.....	15
2.1 Data set: Aromatic and aliphatic amino acids.....	15
2.2 Computational programs	16
2.3 Computational calculations.....	16
2.3.1 Optimization.....	16
2.3.2 Thermodynamical study and intrinsic reaction coordinates (IRC).....	17
2.3.3 Geometric rearrangement.....	18
2.3.4 Electronic study and natural bond orbital (NBO) analysis.....	19
3. Results and discussion	21
3.1 Optimization results.....	21
3.2 Thermodynamic results.....	22
3.3 Geometric results	25
3.4 Electronic results.....	26
3.5 Inhibition results	29
4. Conclusions.....	31
5. Bibliographic references.....	33
A. Appendix: Methodology calculations.....	36
B. Appendix: Calculations results.....	37
C. Appendix: Miscellaneous.....	52

ÍNDICE DE TABLAS

Table 3-1: Wiberg bond analysis, evolution percent and synchronicity of C1-H5 cleavage and H5-O6 formation of aromatic compounds.	29
Table 3-2: Wiberg bond analysis, evolution percent and synchronicity of C1-H5 cleavage and H5-O6 formation of aromatic compounds.	29
Table A-1: Main code lines for Gaussian 16 calculations.	36
Table A-2: Thermal corrections of predicted thermodynamical results in gaseous phase to aqueous solution.	36
Table B-1: Thermodynamic activation parameters of racemization, activation energy, enthalpy, Gibbs free energy and entropy at 383.45 K.	37
Table B-2: Reaction works of H cleavage for racemization in kcal mol ⁻¹	40
Table B-3: Square correlation coefficient R ² and slope m of linear regression between NBO charges of reactant (R), transition state (TS), and intermediate (I) and experimental energy of activation.	49

ÍNDICE DE FIGURAS

Figure 2-1: Racemization mechanism with a carbanion intermediate.	15
Figure 3-1: Theoretical activation energies vs experimental activation energies of racemization.	21
Figure 3-2: IRC energy profiles for racemization of aromatic compounds.	23
Figure 3-3: IRC energy profiles for racemization of aliphatic compounds.	23
Figure B-1: Hammett σ plot using ΔG for calculations of kinetic constants.	37
Figure B-2: Hammett σ plot using ΔH for calculations of kinetic constants.	38
Figure B-3: IRC electronic flux profile for racemization of aromatic compounds.	38
Figure B-4: IRC electronic flux profile for racemization of aliphatic compounds.	39
Figure B-5: IRC reaction force profile for racemization of aromatic compounds.	39
Figure B-6: IRC reaction force profile for racemization of aliphatic compounds.	40
Figure B-7: Hammett σ plot using W_2 for calculations of kinetic constants.	41
Figure B-8: Hammett σ plot using W_3 for calculations of kinetic constants.	41
Figure B-9: Hammett σ plot using W_{23} for calculations of kinetic constants.	42
Figure B-10: IRC breaking of CH bond profile for racemization of aromatic compounds.	42
Figure B-11: IRC breaking of C1-H5 bond profile for racemization of aliphatic compounds.	43
Figure B-12: Bond length difference from reactant to transition state. H5-O6 formation length diminishes and C1-H5 cleavage length increases.	43
Figure B-13: Bond length difference from transition state to product. H5-O6 formation length diminishes and C1-H5 cleavage length increases.	44
Figure B-14: Bond length difference from reactant to product. H5-O6 formation length diminishes and C1-H5 cleavage length increases.	44

Figure B-15: IRC C1-H5-O6 bond angle profile for racemization of aromatic compounds...	45
Figure B-16: IRC C1-H5-O6 bond angle profile for racemization of aliphatic compounds...	45
Figure B-17: IRC N3-C1-C2-C4 dihedral angle profile for racemization of aromatic compounds.	46
Figure B-18: IRC N3-C1-C2-C4 dihedral angle profile for racemization of aliphatic compounds.	46
Figure B-19: Central carbon NBO charge profile for racemization of aromatic compounds.	47
Figure B-20: Central carbon NBO charge profile for racemization of aliphatic compounds..	47
Figure B-21: Central carbon NBO charge profile for racemization of aliphatic compounds..	48
Figure B-22: Central carbon NBO charge profile for racemization of aliphatic compounds..	48
Figure B-23: Bond length comparison between the C1-H5 bond and H5-O6 across IRC calculations.....	49
Figure B-24: Wiberg bond index comparison between the C1-H5 bond and H5-O6 across IRC calculations.	50
Figure B-25: IRC dipole profile for racemization of aromatic compounds.....	50
Figure B-26: IRC dipole profile for racemization of aliphatic compounds.....	51
Figure C-1: Aromatic amino acids.....	52
Figure C-2: Aliphatic amino acids.....	52
Figure C-3: N3-C2-C1 (red) and C2-C1-C4 (blue) planes considered in dihedral angle calculations.....	52

1. INTRODUCTION

Racemization is the reaction that converts an enantiomer into its mirror image through a process called chiral inversion (Ballard et al., 2019), that is, only the chiral center structure is affected through the reaction. The more complex a molecule gets, the higher their tendency to racemize is. This makes biomolecules such as medicine and food supplements (Marcone et al., 2020) prone to racemization (Chen, Leinisch, et al., 2019), given their many chiral atoms. Additionally, when one or more active sites of the molecule are either a chiral atom or any group bonded to it, it is said that the compound is optically active if one enantiomer retains the activity while the other loses it. Therefore, medicine can lose a significant amount of efficiency after undergoing racemization (S. W. Smith, 2009). The new enantiomer can even lead to negative side effects such as carcinogenicity and teratogenicity (Bastings et al., 2019) since the originally inactive site can turn active towards different body receptors.

Even though regioselective reactions that can produce high concentrations of a single enantiomer (Mann et al., 2021) have been studied to increase conversion of optically active compounds in drug design processes (Yan et al., 2021), pure enantiomeric products can be racemized in a different environment because factors such as pH, temperature, catalysts, enzymes, and substrate structure have shown to allow different racemization rates (Hättasch et al., 2021). Hence, even if a regioselective process allowed an enantiomeric pure product, it can be racemized after being ingested. These turns many plant designs non-profitable (Harriehausen et al., 2021) given that chiral specific chromatography, the usual method for enantiomeric purification, requires high costly and functionalized stationary phases (Huang et al., 2021). Moreover, it has been found that proteins and system enzymes may be spontaneously racemized in the body environment (Dyakin et al., 2021), leading to neurological and hormonal diseases, as well as accelerated protein aging.

Another issue of racemization is that little is known about its mechanism. Reaction mechanisms indicate what products will be formed and what geometric rearrangements occur in the reactants, transition states, and intermediate structures to reach the final product (Cuesta, Rincón, et al., 2021), as well as electron transitions to form or break bonds. However, the standard experimental methods to study mechanisms are harder to apply to racemization. Polarimeters are used to assess the presence and concentration of enantiomers by measuring the amount of light absorbed by a sample and the direction it is being polarized (Meinard et al., 1985). This analytical technique follows from the observation that opposite enantiomers polarize light in different directions; nevertheless, complex systems of multiple chiral centers, which are common in large biomolecules and organic solvents (Meinard et al., 1985), can interfere with the polarimeter measure by creating a varying background.

This in addition to the dependence of racemization on many control variables has led to a wide interpretation of experimental results (Brewer et al., 2016; Broberg et al., 2021) with no clear mechanism as a solution. Sivakua and Smith (1983) found that aromatic amino acids, which all have a chiral carbon center prone to suffer racemization, show to racemize with lower activation energies than aliphatic amino acids. Aromatic amino acids have an aromatic ring directly bonded to the chiral carbon (a phenyl group) (Marcone et al., 2020), while aliphatic amino acids have either an indirectly bonded aromatic group, or no aromaticity at all. A carbanion intermediate was proposed to be a key element in racemization, given that aromaticity can distribute and stabilize the localized electron density such as the lone electron pair of the carbanion (Dudek et al., 2022). The Hammett analysis performed in this study also showed that negative charge was being built on by changing the substituent group in the aromatic ring (G. G. Smith & Sivakua, 1983). Still, these aren't finite results, and only work in the aromatic and aliphatic amino acids system, so carbocation and free radical intermediates

have also been proposed for the different racemization mechanisms, as well as concerted pathways.

Other possibilities to study racemization experimentally are limited given the need to purify the enantiomers to measure their polarimeter lectures. Not only are the chiral chromatographic columns high costly, but the intermediate points in the reaction are impossible to purify and study (Harriehausen et al., 2021). Thus, the advantages of computational chemistry are heavily induced by a decrease in experimental equipment cost. Furthermore, complex systems can be easily modelled in computational programs (Planas et al., 2021), including large biomolecules in medicine and body systems (Javierre et al., 2017). The short-lived structures that occur through the reaction, such as transition states and intermediates (Cuesta, Rincón, et al., 2021), can also be closely studied through computational methods. The structural intricacies and rates of the racemization mechanism can be studied simultaneously for different amino acids too (Zeng et al., 2017), making this methodology suitable to study the effect of aromaticity.

The level of theory or computational method has a great impact on the kind of results that can be obtained, as well as the type of systems to be studied. *Ab initio* algorithms try to solve calculations from the Schrödinger equation only (Pokluda et al., 2015), resulting in a wave function to describe the electron distribution on the compounds, and hence, the system energy. Density functional theory (DFT) assumes a correlation between the system energy and the electron density (Pokluda et al., 2015), giving a simplification to the Schrödinger equation that would require only a mapping of the electron distribution across the molecules. in a molecule such as aromaticity and the substituent effect (Chen, Li, et al., 2019).

DFT calculations have been proven effective in the study of reaction mechanisms. For instance, the reaction mechanism of bi-ATDO fast amide cleavage through an intramolecular nitrogen nucleophilic attack was elucidated(Cuesta, Rincón, et al., 2021), as well as the effect of

the nucleophilic nature in the degradation mechanism of chloroacetanilide herbicides (Cuesta, Torres, et al., 2021). Proton transfer between amide dimers has also been studied to better understand biological enzymatic systems (Inostroza-Rivera et al., 2014). The methodology has also helped discriminate between two possible mechanisms for the alkyl *t*-butyl ethers thermal decomposition catalyzed by hydrogen chloride (Cuesta, Mora, Meneses, et al., 2022). These studies utilize the *ωb97xd* method in DFT calculations as it allows to better approximate the far weak interactions, making it the suitable algorithm for this project.

An initial guess structure for the stationary points must first be optimized using the selected level of theory (Pokluda et al., 2015). After these structures have been validated with experimental data, distinct properties can be predicted from the computational model to describe the work done through the reaction, steric effects, point charge of atoms, among others (Goerigk & Sharma, 2016). This will help to characterize the mechanism and the most relevant driving factors of it, so by neutralizing those factors, an inhibition method for racemization could be found (Takahashi et al., 2016). If these methods are applied in the pharmaceutical industry, product quality and price will increase (Orlandin et al., 2022) as more efficient plant designs and regioselective processes are readily available. This follows from medicine having close to 100% of its original activity and fewer or no negative side effects (Sturabotti et al., 2023). Since amino acids are the building blocks of many relevant biomolecules (Prabhu et al., 2015), understanding their mechanism of racemization may elucidate the pathway to study more complex biological systems and drugs (Chamakuri et al., 2022), as well as optimization methods for their synthesis.

2. METHODOLOGY

2.1 Data set: Aromatic and aliphatic amino acids

The reaction mechanism involved in the amino acids racemization imply the formation of a carbanion intermediate according to the process described in Figure 2-1 (G. G. Smith & Sivakua, 1983). The electron-positive hydrogen from the chiral carbon is attacked by a hydroxyl group considering that the reaction will be studied in basic media. Additionally, the reaction is expected to be symmetric, that is, there aren't any reactants such as enzymes that would turn the reaction regioselective; therefore, the same energy levels would be expected from both enantiomers and their respective transition states. It follows that every property and change would be mirrored after the intermediate, so only the reactant to transition state step is evaluated.

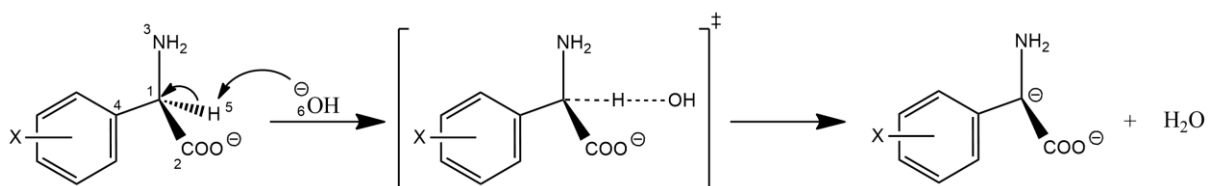


Figure 2-1: Racemization mechanism with a carbanion intermediate.

The data set used for this study was obtained from the article reported by Sivakua and Smith (1983), which involve 11 different amino acids. Aromatic amino acids, such as phenylglycine, have an aromatic ring linked directly to the chiral carbon, which allows stabilization by resonance of the carbanion negative charge. Five additional phenylglycines are studied, which differ by their substituent on the aromatic ring. In contrast, alanine, valine, leucine, isoleucine, and phenylalanine, which have either indirectly linked aromatic rings or none at all, are taken as the aliphatic amino acids sample. Both the aromatic and aliphatic amino acid structures are gathered in Figure C-1 and Figure C-2 respectively.

2.2 Computational programs

The calculations will be conducted through Gaussian 16, a program with access to different computational tools and methods, such as semi-empiric, *ab initio*, and DFT methods (Frisch et al., 2016). The chosen level of theory is *ωb97xd/6-311++g(d,p)*, because of its better reliance over other functionals to study the effect of weak interactions such as the substituent effect due to aromaticity (Chen, Li, et al., 2019), and the same method is used in all stationary points of the reaction. The input files for the calculations can be managed with GausView6, a software used to visualize compound structures, as well as other results from Gaussian 16 calculations (Keith et al., 2016), such as intrinsic reaction coordinates (IRC) diagrams, bond lengths, and angles, as well as atomic charge values. The amino acid models were done using predetermined structures available in GausView6, and the substituted aromatic amino acids were drawn by hand from phenylglycine.

2.3 Computational calculations

2.3.1 Optimization

Optimization calculations minimize the systems energy to get the most stable structure of a stationary point such as reactant, transition state, intermediate, and product, given an initial guess (Pokluda et al., 2015). Optimization is necessary to know the plausible molecular structures of reactants, therefore reaching an equilibrium state described by the corresponding level of theory. Once optimized, frequency calculations are performed to predict the vibrating modes of the molecule bonds and, therefore, its energy (Chen, Li, et al., 2019), which can then be used to determine enthalpy, entropy, and free energy by employing the thermodynamic statistical approaches in gas phase. Given that all structures near a transition state have less energy than it, that is, a maximum is reached, imaginary frequencies must be allowed to find these negative second derivative values (Cuesta, Rincón, et al., 2021). All the main codelines

are shown in Table A-1. The activation energy predicted by the frequency calculations can be obtained through the enthalpy difference between the transition state and the reactant, but it would be representative of gaseous reactants. The reaction takes place in aqueous media, so additional energy contributions must be considered in the calculations of thermodynamical results (Rastelli et al., 1995), and they are present in Table A-2.

2.3.2 *Thermodynamical study and intrinsic reaction coordinates (IRC)*

The influence of the aromatic substituent nature on the tendency to form a charged intermediate can be studied with the Hammett equation. It implies a linear correlation between the free energy of a reaction and an experimental substituent parameter σ (G. G. Smith & Sivakua, 1983), where the proportionality constant ρ depends on the type of reaction. The Hammett equation is:

$$\log \frac{k}{k_0} = \rho \sigma$$

where k_0 is the rate of the reaction with a not-substituted reactant, k is the rate constant for the case of a specific substituent, and σ is the respective substituent constant, which depends on the functional group nature and its position in the aromatic ring. It has been found experimentally that positive reaction constant values show a negative charge being built through the reaction, and a high absolute value would imply sensitivity towards substituents (G. G. Smith & Sivakua, 1983).

Intrinsic reaction coordinates (IRC) calculate the system energy E along the normalized reaction coordinates ξ starting from the transition state. Stable structures are present on either side of the transition state, so IRC calculations look for energy plateaus as termination points. The main code line for an IRC calculation is shown in Table A-1. Additionally, derivating the energy profile gives the reaction force F defined as (Inostroza-Rivera et al., 2014):

$$F(\xi) = -\frac{dE}{d\xi}$$

The critical points of the reaction force profile naturally separate the energy IRC into four regions. While the extreme regions correspond to structural rearrangement, and the centered regions to electronic reordering, the first two stages correlate to reaching the transition state, and the last stages to relaxation. Integration of the reaction force in each stage gives the reaction work required for each one, according to the following equation (Cuesta, Mora, Meneses, et al., 2022):

$$W_x = -\int_i^j F(\xi)d\xi$$

Another parameter is the chemical potential μ , which is calculated alongside the energy, and allows to obtain the IRC of the electronic flux J , defined as (Cuesta, Mora, & Márquez, 2022):

$$J(\xi) = -\frac{d\mu}{d\xi}$$

Positive and negative electronic flux values in the transition region correlate to bond forming and breaking respectively being more significant in the reaction.

2.3.3 Geometric rearrangement

Bond lengths between atoms can be obtained from the optimized structures to understand which species displace the most due to steric effects or electronic repulsion (Türker et al., 2009), such as the C₁-H₅ bond breaking and the H₅-O₆ bond forming. The angle between these three atoms can also be studied to determine the collision geometry for the given reaction (Da et al., 2019). Finally, the dihedral angle between the N₃-C₂-C₁ plane and the C₂-C₁-C₄ plane (Figure C-3) allows to determine the molecular geometry of the species (Türker et al., 2009), which would be expected to be pyramidal for the carbanion intermediate. The evolution of bond lengths, angles, and dihedral angles can also be studied through IRC calculations, and

lengths of relevant reacting bonds can be compared to study the symmetry of the reaction (De Souza et al., 2016).

2.3.4 *Electronic study and natural bond orbital (NBO) analysis*

The results of DFT calculations are based on electron wave behaviour, and the properties of the system as a whole are taken from the wave function. Therefore, natural bond orbital (NBO) calculations are necessary to find a localized representation of the electrons in each of the atoms in order to estimate the point charges (Cuesta, Rincón, et al., 2021). The Wiberg bond index (WBI) shows the average number of electron pairs between atoms, indicating the bond strength (Cuesta, Rincón, et al., 2021), and can be obtained from the NBO results. The evolution of the NBO charges and the WBIs across the reaction, a novel method to study synchronicity not reported in the literature, can also be obtained from IRC calculations with the main code line of Table A-1. Given that the highest changes in WBI values show the bonds that break or form “the most”, relevant bond transitions can be determined through the NBO analysis, as well as the symmetry of the reaction according to the reactive bonds. The percentage evolution $\%Ev_i$ of a bond i across the reaction is defined as (Cuesta, Mora, Meneses, et al., 2022):

$$\%Ev_i = \left[\frac{B_i^{TS} - B_i^R}{B_i^I - B_i^R} \right] \times 100$$

where the values of B_i are the respective Wiberg bond indexes of the reactant (R), transition state (TS) and intermediate (I). Percentage evolutions below 50% would confirm an early transition state, while values over 50% correspond to a late-occurring reaction. If more than one bond is involved in the reaction, the synchronicity Sy can be defined as (Cuesta, Mora, Meneses, et al., 2022):

$$Sy = 1 - \frac{\left[\sum_{i=1}^n \frac{[\%Ev_i - \overline{\%Ev}]}{\%Ev} \right]}{2n - 2}$$

where n is the number of bonds and $\overline{\%E\nu}$ is the average percentage evolution between all involved bonds. Synchronicity shows compares the extent to which bond-breaking and forming processes have taken place in the transition state, giving thus a symmetry parameter to the reaction. A different method of calculating point charges, the Mulliken population analysis, lacks on representing weak interactions correctly (Gómez-Jeria, 2009), so it will also be studied and compared to the NBO results as contrast on the aromaticity effect. Moreover, the dipole of the whole molecule can be calculated through IRC analysis and would show the effect of other point charges and electron concentration in the molecule aside from the active center.

3. RESULTS AND DISCUSSION

3.1 Optimization results

The theoretical activation energy at a temperature of 110.3 °C for the evaluated amino acids is tabulated next to the experimental results obtained by Smith & Sivakua (1983) in Table B-1, as well as the enthalpy, free energy and entropy of activation. The plot of experimental vs calculated activation energy E_A (Figure 3-1) shows a tendency of aromatics having lower activation energy than aliphatic amino acids, although the nitro-substituted phenylglycine seems to be the furthest away from its experimental value. Also, while phenylalanine is not as close in energy to the other aliphatic amino acids as the aromatics are between them, its activation energy remains at a higher value than that for aromatics. Based on these results, the optimized model is validated and it will be sufficient to obtain theoretical information on the mechanism (Cuesta, Mora, Meneses, et al., 2022), especially after corrections on the activation energy were done. The corresponding transition states for valine and alanine were not able to be optimized, so their data would be scrapped from the optimization analysis.

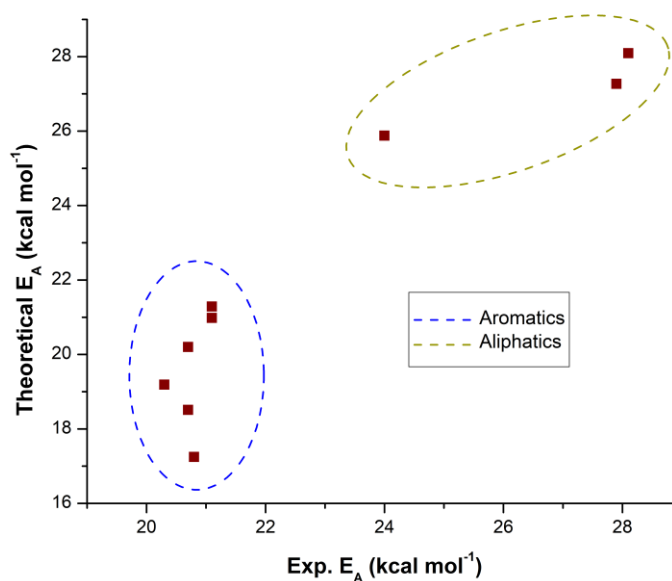


Figure 3-1: Theoretical activation energies vs experimental activation energies of racemization.

3.2 Thermodynamic results

Figure B-1 shows the logarithm ratio of the kinetic constants, which is proportional to the free energy, of substituted aromatics, to the Hammett parameters of each substituent. As expected, a linear correlation of positive slope is followed by the data, so the tendency follows the formation of a negative charge through the reaction. The values are however not too precise, so by considering the limitation of entropy calculations of DFT methods as well as the lack of reordering done in the proposed mechanism, a second Hammett plot using only the enthalpy instead of the free energy was done and is shown in Figure B-2, obtaining the correlation coefficient has a value of 0.997, so the values are more accurate when using enthalpy instead of free energy, which further proves the accuracy of the optimization results. Then, the effect of the substituents agrees with the formation of a carbanion intermediate for aromatic amino acids, and the sensitivity of the charge stability towards the substituents is high considering the high slope value of 2.33 from the correlation.

The energy profiles of aromatics are graphed together in Figure 3-2, while aliphatic amino acids are shown in Figure 3-3. The transition state is always closer in energy to the intermediate than to the reactant, so according to Hammond's postulate, the structure of both species will also be similar. More specifically, activating groups in aromatic amino acids destabilize the intermediate, and deactivating groups stabilize it. Given that the reaction is prone to a negative charge, deactivating groups would direct resonant electron movement toward the ring and away from the negative charge, resulting in a stabilizing effect. Nevertheless, aliphatic transition states and intermediates barely differ in energy, occurring very late in the reaction. Hence, aliphatic compounds don't show a tendency towards the carbanion, and if so, its structure is highly unstable in addition to variations on aliphatic structure not having an effect on its stability. It should be noted that phenylalanine follows a

very similar tendency to the other aliphatics, further proving its behavior as an aliphatic despite the aromatic ring.

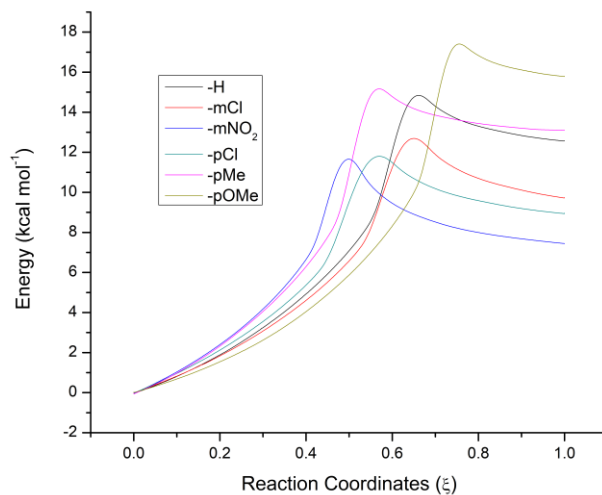


Figure 3-2: IRC energy profiles for racemization of aromatic compounds.

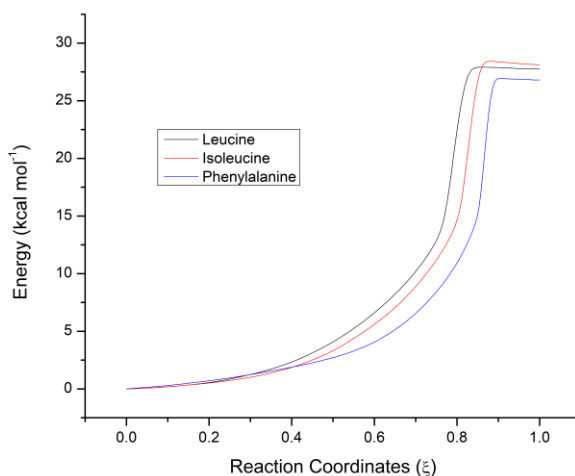


Figure 3-3: IRC energy profiles for racemization of aliphatic compounds.

Electronic flux values are negative for all aromatic and aliphatic amino acids in the transition state region, as shown in Figure B-3 and Figure B-4 respectively. The C-H bond breaking is thus a more relevant transition than the O-H bond forming with the attacking group; moreover, electronic effects that may alter the acidity of the central carbon are more relevant than the basicity of the attacking group. Indeed, aliphatic amino acids are driven by the acidity

of the central carbon more than aromatics because they reach higher absolute values of electronic flux. However, electronegative aromatic substituents show less acidity on the chiral carbon than other activating groups. This could be explained by resonance being more effective than inductive electron withdrawal at stabilizing the carbanion intermediate.

Similarly, reaction force diagrams are shown for aromatic and aliphatic amino acids in Figure B-5 and Figure B-6 respectively. Furthermore, the integration of the diagrams to obtain the reaction works are shown in Table B-2. The higher total values for the external regions show that more energy is needed in structural rearrangement than electronic reordering for all species. Therefore, the energy needed for species to come close to react is more significant, and a more detailed observation of the data for aliphatic amino acids shows that the highest contributor is the first stage. In fact, the last stage is negligible, which can be contributed to aliphatic amino acids not having an intermediate structure in their true mechanism.

Conversely, aromatic amino acids require less energy for electronic reordering and structural rearrangement than aliphatic compounds, given the stabilization effect from aromatic resonance. Activating groups also increase the energy required for all stages in comparison to deactivating groups, which was an expected result for the middle stages due to resonance stabilization, yet it proves that the substituent also decreases the energy for the attacking group to come together with the chiral carbon. This could be contributed to electronic density repulsion against the hydroxyl group being distributed by aromaticity induction.

To further prove this, the reaction works were plotted against Hammett parameters to see if any of the stages has the highest contribution to the formation of the carbanion intermediate. The highest correlation coefficients were obtained when using W_2 with a value of 0.67 (Figure B-7), and W_3 with a value of 0.63 (Figure B-8). While the correlation is not high, the positive slope in the first case shows a negative charge being built in the transition state as the acid hydrogen bond is broken, but the negative slope for the third stage shows relaxation

of that negative charge towards the intermediate. Hence, aromaticity only takes place in the structure with a full formed negative charge, and not in partially charged stationary points such as the transition state. Furthermore, the distribution utilizing W_1 did not follow a clear linear tendency, so the effect of aromaticity is attributed to the electron reordering only, and not to the structural rearrangement.

3.3 Geometric results

The displacement between the chiral carbon and its acid hydrogen increases as the bond breaks as shown in Figure B-10 and Figure B-11. Even though the displacement is higher in aromatic amino acids with a deactivating group, the difference is very small. Besides, the aliphatic displacement is similar to that done by aromatics, so the displacement of the bond forming between the hydroxyl group and the acid hydrogen should have greater implications. The absolute differences between each stationary point are shown in Figure B-12 (reactant to transition state), Figure B-13 (transition state to intermediate), and Figure B-14 (reactant to intermediate). Aliphatic compounds show an important increase in the distance between atoms, which is contributed to the repulsion in the first stages of the reaction playing a major role in aliphatic racemization than in aromatics. The difference could also imply that the steric effects of the nucleophile are more relevant in aliphatic amino acids, given that the distance of the hydroxyl group, the most displaced bond, would be higher.

The IRC evolution of the bond angle between the chiral carbon, the acid hydrogen, and the hydroxy group oxygen are shown in Figure B-15 and Figure B-16 for aromatic and aliphatic amino acids respectively. Aromatic compounds have angle variations of less than 3° , so the reaction follows a linear path and would require very little energy in geometric rearrangement. Aliphatic amino acids show a great angle displacement, mainly phenylalanine. When looking at the IRC animations, this is due to a heavy rotation performed by the attacking hydroxy group,

so the attraction of the hydroxyl hydrogen and the formation of negative charge is needed to replace the aromatic stabilization of said charge. This would also help to describe the higher need of structural rearrangement energy of aliphatic racemization as described in the reaction work analysis.

This observation is further proved by the IRC calculation of the dihedral angle between two planes involving the chiral carbon and its neighboring bonds. Figure B-17 shows that no changes in the molecular geometry of the central carbon happen until the late reaction stages, so small energy for structure modifications is required. The angle increases as the previously tetrahedral develops into a pyramidal composition, where the 20° to 30° difference from the 180° planar composition proves that the structure is being repelled by a lone electron pair, thus indicating the presence of a carbanion intermediate. The more the deactivating nature of the group, the less repulsion is given by the electron pair that is being distributed through resonance as the angle approaches 180° . Aliphatic amino acids show instead heavy dihedral evolution from the early reaction stages as shown in Figure B-18, and all result in similar angular intermediates that are less prompt to form resonance structures to favor racemization.

3.4 Electronic results

Figure B-19 and Figure B-20 show the IRC evolution of the NBO charge of the chiral carbon. The negative charge is stabilized in the intermediate for aromatics, but a highly negative charged transition state does happen. Thus, equilibrium must take place between the transition state and the intermediate for the aromatic resonance to deactivate the carbanion center. Additionally, the value of the most negative NBO charge reached remains similar for all species, and no tendency in the carbanion charge value due to changes of the activation capacity of the substituent is followed. Aliphatic amino acids do reach a similar charge in the transition region, so only the nitro-substituted phenylglycine has a more positive intermediate

in comparison to all species. This could be addressed by deactivating substituent capacity having a bigger impact than electronegativity attraction of the electron density.

Mulliken charge IRC analysis is shown too in Figure B-21 and Figure B-22. While the same falling of the charge value in the first regions of the reaction is observed as with the NBO model, the negative charges don't stabilize for any aromatic species. The neighboring group orbitals and aromaticity being the main cause of the stabilization could contribute to this observation because Mulliken calculations don't consider weak interactions (Gómez-Jeria, 2009). Adding to the contrast, Mulliken calculations do show a relative difference in the charge reached in the transition region, which directly contradicts the previous statement. Since Mulliken analysis is dependent on the basis used, and DFT needs the assumption of a relation between electronic density and the system energy, Mulliken results are not reliable for weak interactions.

The linear correlation between the NBO charges transitions and the experimental energy of activation for all amino acids was studied. Table B-3 shows that while atoms such as the carboxyl carbon and the amine nitrogen have high correlations with the charges, their slopes are close to zero and their tendency is rendered to a simple constant function. The only correlations with noteworthy parameters are the chiral carbon and the acid hydrogen relating to their charges in the reactant structure. They have similar valued slopes with opposite signs; hence, their point charge evolution would have the most focal influence on the contrast of activation energy, with correlation coefficients of approximately 0.9.

In the present work, we introduce the calculation of the Wiberg bond indexes in the stationary points of all species involved in the reaction coordinates, synchronicity and evolution percentages of aromatic amino acids were calculated in Table 3-1. The percentage evolution values of aromatic amino acids increase from around 57% to 68% when increasing the activating capacity of the substituents, thus causing for the transition state to occur in late

stages of the reaction. Nonetheless, the system remains highly symmetric for all substituents, which could be likely due to activating groups destabilizing the carbanion, consequently increasing the repulsion between reactants, yet the extent of bond breaking and forming remains the same. Similarly, Table 3-2 shows that aliphatic amino acids have higher evolution percentages than aromatics, so their transitions occur later in racemization, but they stay at a comparable synchronicity.

Analyzing synchronicity can also be done by observing the relation between the bond length evolution of the C₁-H₅ rupture and H₅-O₆ bonding across the reaction coordinates (Figure B-23). The graph follows a path below linearity, thus implying that the reaction's asymmetry is driven by the forming H₅-O₆ bond (De Souza et al., 2016), and the distinct curves between aromatic and aliphatic amino acids can also be attributed to the further displacement of these atoms (Figure B-14). Nevertheless, studying the relation of the WBIs of the same bonds instead of the lengths do prove high synchronicity in the reaction as shown in Figure B-24. Even aliphatic amino acid curves are indistinguishable from those of aromatics, as expected from the synchronicity results in Table 3-1 and Table 3-2. Therefore, bonding strength is not affected by aromaticity, rather only the point charge on each atom, and the contrast with bond length could be attributed to the orientation of the attacking group being more relevant than the bond strengths in all stationary points.

Finally, the dipole IRC evolution of the system is shown in Figure B-25 and Figure B-26 for different amino acids. All aromatic molecules seem to decrease the dipole magnitude, which can be explained in function of the charge distribution through aromatic resonance. While the most activating group, the methoxy substituent, has the highest dipole magnitude, the most deactivating group, the nitro substituent, remains the lowest and most stable dipole. The nature of the solvent in the reaction must then be crucial in helping stabilize the carbanion intermediate. In contrast, isolated charges are observed in aliphatic compounds by an increase

in the dipole magnitude, given their structures don't allow for resonance distribution. Indeed, phenylalanine has a high dipole even with an aromatic ring linked to its structure. The relevance of whether resonance structures can be in equilibrium through the chiral and beta carbon bond explains this observation, as a high concentration of negative charge due to the aromatic electronic cloud that is not being distributed in phenylalanine would give rise to its high dipole magnitude.

Table 3-1: Wiberg bond analysis, evolution percent and synchronicity of C1-H5 cleavage and H5-O6 formation of aromatic compounds.

Compound	Phenylglycine		mCl-Phenylglycine		mNO ₂ -Phenylglycine	
	C ₁ -H ₅	H ₅ -O ₆	C ₁ -H ₅	H ₅ -O ₆	C ₁ -H ₅	H ₅ -O ₆
Reactant	0.8114	0.0446	0.7943	0.0544	0.7899	0.0566
T. State	0.3396	0.4344	0.3546	0.4171	0.3675	0.4059
Product	0.0809	0.6602	0.0782	0.6639	0.0549	0.6878
%Ev	64.586	63.320	61.402	59.508	57.469	55.339
Sy	0.990105548		0.984333404		0.98111532	
Compound	pCl-Phenylglycine		pMe-Phenylglycine		pOMe-Phenylglycine	
	C ₁ -H ₅	H ₅ -O ₆	C ₁ -H ₅	H ₅ -O ₆	C ₁ -H ₅	H ₅ -O ₆
Reactant	0.7751	0.0666	0.8092	0.0463	0.8408	0.0278
T. State	0.3505	0.4203	0.3305	0.4424	0.3254	0.4472
Product	0.0781	0.6625	0.0787	0.6619	0.0891	0.6521
%Ev	60.918	59.356	65.530	64.344	68.565	67.179
Sy	0.987007776		0.990862473		0.989794408	

Table 3-2: Wiberg bond analysis, evolution percent and synchronicity of C1-H5 cleavage and H5-O6 formation of aromatic compounds.

Compound	Leucine		Isoleucine		Phenylalanine	
	C ₁ -H ₅	H ₅ -O ₆	C ₁ -H ₅	H ₅ -O ₆	C ₁ -H ₅	H ₅ -O ₆
Reactant	0.8856	0.0058	0.8874	0.0055	0.8967	0.0040
T. State	0.2220	0.5332	0.2394	0.5112	0.2453	0.5213
Product	0.1113	0.6239	0.1060	0.6285	0.1206	0.6271
%Ev	85.703	85.326	82.928	81.172	83.932	83.020
Sy	0.997794431		0.989297196		0.994536776	

3.5 Inhibition results

According with the literature, the racemization reaction for the studied amino acids only occurs in basic media, and as expected none transition states for a reaction in neutral media were able to be optimized. Therefore, no results for activation energy comparison with the

reaction performed in basic media were obtained. A distinct mechanism could take place by the change in pH, and the structure of a carbanion intermediate is too unstable to have a recognizable minimum in a potential function. This, however, is not a complete result because the optimum initial guesses for the structures could have been missed. The correct path to reject the carbanion as a mechanism step would be to find the true mechanism with an accurate validation.

Besides, it was awaited for the hydroxyl group to play a vital role in the geometric movement of the reactants during the first stage of reaction, since repulsion between the negative charges of the carbanion and the nucleophile would be stabilized by aromatic resonance. Indeed, it was found that the attacking group in aliphatic racemization executes notable rotations and displacements to reach the transition state, giving rise to more energy required in the structural rearrangement. If a similar mechanism would be obtained for a neutral water molecule as the nucleophile, it would be expected to have an increase in energy in the same reaction stages, as aromatic stabilization would no longer reduce repulsion between the compounds. The amine group should also be considered as protonated for this reaction, so further studies to understand the effect of the additional positive charge should follow.

4. CONCLUSIONS

From the optimization and frequency results it was well validated the obtained transition states for the mechanism in function of the correlation with the experimental results and the reactivity tendency found. Hence, more amino acids should be added to increase the accuracy of the curve. Both aliphatic amino acids could increase the accuracy of the curve in the region where leucine and isoleucine lie. There's also a wide gap between the aromatic and aliphatic structures, and only phenylalanine could be related to this zone. More aliphatic amino acids that have an aromatic ring indirectly linked to the chiral carbon should be studied to improve the accuracy of the correlation in this region.

Thermodynamic results seem to highlight the acidity of the hydrogen bonded to the chiral carbon as the main driving factor of the reaction. As expected, aromatic resonance showed to increase the acidity by stabilizing the intermediate carbanion charge (the conjugated base), thus requiring less energy for both geometric rearrangements of the amino acid and the nucleophile, as well as electronic reordering due to a more stable distribution of the electronic density. Aliphatic amino acids did more work during these transitions than aromatics and could even create additional repulsion as the transition state showed a similar or even lower charge than the intermediate. The energy IRC in Appendix also implied that the intermediate structure is too similar in energy and structure to the transition state. A different mechanism for aliphatic amino acids should then be examined in the future, which could involve a concerted or free radical mechanism. The transition state, however, should not be so far apart from the one in the carbanion mechanism, as the predicted activation energies are close to those found experimentally.

When studying specifically the effect of aromatic substituents, the Hammett analysis showed that the carbanion stability is sensitive towards substituents, due to its slope value of

over 2. The increase in the correlation coefficient when using the free energy instead implies that the study could be improved by optimizing more aromatic structures of different substituents and varying not only the functional group, but their ring position as well. Particularly, deactivating groups show to distribute the negative carbanion charge more than activating groups. This follows from observations such as the carbanion charge turning less negative value in the path from the transition region to the intermediate, the dipole magnitude declining in aromatic amino acids, and both the reaction works and activation energies decreasing as the deactivating capacity of the substituent increases. This variability can be attributed to both the structural rearrangement towards a pyramidal carbanion, and a different electronic distribution to form a stable negative charge.

Lastly, similar conclusions can be reached to discuss the mechanism in neutral pH as those for the non-optimized amino acids. The literature predicts that a change in pH may lead to a different mechanism, thus resulting in the transition state before the carbanion intermediate not optimizing. Similarly, the lack of aromatic structures to stabilize the intermediate allowed to predict that certain aliphatic amino acids optimization didn't reach a transition state. Looking into a free radical structure or a concerted reaction with two nucleophiles are proposed as possible mechanisms, since the decrease of negative charge in their geometries would have a better chance of reacting with a water molecule, given the nature of the nucleophile is relevant in racemization. Likewise, further decreasing the pH could influence the mechanism as well, a carbocation being likely given the opposite characteristics of the hydronium and hydroxide ions.

5. BIBLIOGRAPHIC REFERENCES

- Ballard, A., Narduolo, S., Ahmad, H. O., Cosgrove, D. A., Leach, A. G., & Buurma, N. J. (2019). The problem of racemization in drug discovery and tools to predict it. In *Expert Opinion on Drug Discovery* (Vol. 14, Issue 6, pp. 527–539). Taylor and Francis Ltd. <https://doi.org/10.1080/17460441.2019.1588881>
- Bastings, J. J. A. J., van Eijk, H. M., Damink, S. W. O., & Rensen, S. S. (2019). D-amino acids in health and disease: A focus on cancer. In *Nutrients* (Vol. 11, Issue 9). MDPI AG. <https://doi.org/10.3390/nu11092205>
- Brewer, G., Brewer, C., Butcher, R. J., & Zemba, M. (2016). Structural evidence of a ketimine as the product of an amino acid with an aldehyde. An intermediate in the racemization and transamination of amino acids. *Inorganic Chemistry Communications*, 64, 35–38. <https://doi.org/10.1016/j.inoche.2015.12.007>
- Broberg, A., Nord, C., Levenfors, J. J., Bjerketorp, J., Guss, B., & Öberg, B. (2021). In-peptide amino acid racemization via inter-residue oxazoline intermediates during acidic hydrolysis. *Amino Acids*, 53(3), 323–331. <https://doi.org/10.1007/s00726-021-02951-7>
- Chamakuri, S., Tang, S. A., Tran, K. A., Guduru, S. K. R., Bolin, P. K., Mackenzie, K. R., & Young, D. W. (2022). A Concise Synthetic Method for Constructing 3-Substituted Piperazine-2-Acetic Acid Esters from 1,2-Diamines. *Molecules*, 27(11). <https://doi.org/10.3390/molecules27113419>
- Chen, Z., Leinisch, F., Greco, I., Zhang, W., Shu, N., Chuang, C. Y., Lund, M. N., & Davies, M. J. (2019). Characterisation and quantification of protein oxidative modifications and amino acid racemisation in powdered infant milk formula. *Free Radical Research*, 53(1), 68–81. <https://doi.org/10.1080/10715762.2018.1554250>
- Chen, Z., Li, Y., He, Z., Xu, Y., & Yu, W. (2019). Theoretical investigations on charge transport properties of tetrabenzo[a,d,j,m]coronene derivatives using different density functional theory functionals (B3LYP, M06-2X, and wB97XD). *Journal of Chemical Research*, 48(7–8), 293–303. <https://doi.org/10.1177/1747519819861626>
- Cuesta, S. A., Mora, J., & Márquez, E. (2022). GAS PHASE DECOMPOSITION OF T-BUTYL METHYL ETHER CATALYZED BY DIFFERENT HYDROGEN HALIDES: A DFT STUDY. *InfoANALÍTICA*, 10(2), 65–79. <https://doi.org/10.26807/ia.v10i2.237>
- Cuesta, S. A., Mora, J. R., Meneses, L. M., Márquez, E. A., Flores-Morales, V., Rincón, L., Torres, F. J., & Zambrano, C. H. (2022). Unveiling the structure-reactivity relationship involved in the reaction mechanism of the HCl-catalyzed alkyl t-butyl ethers thermal decomposition. A computational study. *International Journal of Quantum Chemistry*, 122(14). <https://doi.org/10.1002/qua.26915>
- Cuesta, S. A., Rincón, L., Torres, F. J., Rodríguez, V., & Mora, J. R. (2021). A computational study of the reaction mechanism involved in the fast cleavage of an unconstrained amide bond assisted by an amine intramolecular nucleophilic attack. *Journal of Computational Chemistry*, 42(12), 818–826. <https://doi.org/10.1002/jcc.26501>
- Cuesta, S. A., Torres, F. J., Rincón, L., Paz, J. L., Márquez, E. A., & Mora, J. R. (2021). Effect of the nucleophile's nature on chloroacetanilide herbicides cleavage reaction mechanism. A dft study. *International Journal of Molecular Sciences*, 22(13). <https://doi.org/10.3390/ijms22136876>
- Da, L. G., He, J., & Hu, L. F. (2019). DFT study on the structure and racemization mechanism of 2-amino-2'-hydroxy-1,1'-binaphthyl. *Journal of Physical Organic Chemistry*, 32(2). <https://doi.org/10.1002/poc.3900>

- De Souza, M. A. F., Ventura, E., Do Monte, S. A., Riveros, J. M., & Longo, R. L. (2016). Revisiting the concept of the (a)synchronicity of diels-alder reactions based on the dynamics of quasiclassical trajectories. *Journal of Computational Chemistry*, *37*(8), 701–711. <https://doi.org/10.1002/jcc.24245>
- Dudek, W. M., Ostrowski, S., & Dobrowolski, J. C. (2022). On Aromaticity of the Aromatic α -Amino Acids and Tuning of the NICS Indices to Find the Aromaticity Order. *Journal of Physical Chemistry A*, *126*(22), 3433–3444. <https://doi.org/10.1021/acs.jpca.2c00346>
- Dyakin, V. V., Wisniewski, T. M., & Lajtha, A. (2021). Racemization in post-translational modifications relevance to protein aging, aggregation and neurodegeneration: Tip of the iceberg. In *Symmetry* (Vol. 13, Issue 3). MDPI AG. <https://doi.org/10.3390/sym13030455>
- Frisch, M., Trucks, G., Schlegel, H., Scuseria, G., Robb, M., Cheeseman, J., Scalmani, G., Barone, V., Petersson, G., Nakatsuji, H., Li, X., Caricato, M., Marenich, A., Bloino, J., Janesko, B., Gomperts, R., Mennucci, B., Hratchian, H., Ortiz, J., ... Fox, D. (2016). *Gaussian 16, Revision C.01*. Gaussian, Inc., Wallingford CT. <https://gaussian.com/g16main/>
- Goerigk, L., & Sharma, R. (2016). The INV24 test set: How well do quantum-chemical methods describe inversion and racemization barriers? *Canadian Journal of Chemistry*, *94*(12), 1133–1143. <https://doi.org/10.1139/cjc-2016-0290>
- Gómez-Jeria, J. S. (2009). AN EMPIRICAL WAY TO CORRECT SOME DRAWBACKS OF MULLIKEN POPULATION ANALYSIS. In *J. Chil. Chem. Soc* (Vol. 54, Issue 4).
- Harriehausen, I., Bollmann, J., Carneiro, T., Bettenbrock, K., & Seidel-Morgenstern, A. (2021). Characterization of an immobilized amino acid racemase for potential application in enantioselective chromatographic resolution processes. *Catalysts*, *11*(6). <https://doi.org/10.3390/catal11060726>
- Hättasch, T., Schmuck, C., & Niemeyer, J. (2021). Triazole groups as biomimetic amide groups in peptides can trigger racemization. *Arkivoc*, *2021*(3), 185–196. <https://doi.org/10.24820/ARK.5550190.P011.484>
- Huang, H., Jin, Y., Shirbhate, M. E., Kang, D., Choi, M., Chen, Q., Kim, Y., Kim, S. J., Byun, I. S., Wang, M., Bouffard, J., Kim, S. K., & Kim, K. M. (2021). Enantioselective extraction of unprotected amino acids coupled with racemization. *Nature Communications*, *12*(1). <https://doi.org/10.1038/s41467-020-20402-x>
- Inostroza-Rivera, R., Herrera, B., & Toro-Labbé, A. (2014). Using the reaction force and the reaction electronic flux on the proton transfer of formamide derived systems. *Physical Chemistry Chemical Physics*, *16*(28), 14489–14495. <https://doi.org/10.1039/c3cp55159h>
- Javierre, G., Fortrie, R., Jean, M., Moraleda, D., Naubron, J. V., & Fotiadu, F. (2017). Racemization and transesterification of alkyl hydrogenophenylphosphinates. *Journal of Molecular Modeling*, *23*(5). <https://doi.org/10.1007/s00894-017-3343-7>
- Keith, T., Millam, J., & Dennington, R. (2016). *GaussView, Version 6*. Semichem Inc., Shawnee Mission, KS. <https://gaussian.com/gv6main/>
- Mann, L., Lang, M., Schulze, P., Halz, J. H., Csuk, R., Hoenke, S., Seidel, R. W., & Richter, A. (2021). Racemization-free synthesis of $N\alpha$ -2-thiophenoyl-phenylalanine-2-morpholinoanilide enantiomers and their antimycobacterial activity. *Amino Acids*, *53*(8), 1187–1196. <https://doi.org/10.1007/s00726-021-03044-1>
- Marcone, G. L., Rosini, E., Crespi, E., & Pollegioni, L. (2020). D-amino acids in foods. In *Applied Microbiology and Biotechnology* (Vol. 104, Issue 2, pp. 555–574). Springer. <https://doi.org/10.1007/s00253-019-10264-9>
- Meinard, C., Bruneau, P., & Perronnet, J. (1985). High-performance liquid chromatograph coupled with two detectors: a UV spectrometer and a polarimeter. Example in the field

- of pyrethroids: identification of enantiomers. *Journal of Chromatography*, 349, 109–116.
- Orlandin, A., Guryanov, I., Ferrazzano, L., Biondi, B., Biscaglia, F., Storti, C., Rancan, M., Formaggio, F., Ricci, A., & Cabri, W. (2022). Carbodiimide-Mediated Beckmann Rearrangement of Oxyma-B as a Side Reaction in Peptide Synthesis. *Molecules*, 27(13). <https://doi.org/10.3390/molecules27134235>
- Planas, F., McLeish, M. J., & Himo, F. (2021). Enzymatic Stetter Reaction: Computational Study of the Reaction Mechanism of MenD. *ACS Catalysis*, 11(19), 12355–12366. <https://doi.org/10.1021/acscatal.1c02292>
- Pokluda, J., Černý, M., Šob, M., & Umeno, Y. (2015). Ab initio calculations of mechanical properties: Methods and applications. In *Progress in Materials Science* (Vol. 73, pp. 127–158). Elsevier Ltd. <https://doi.org/10.1016/j.pmatsci.2015.04.001>
- Prabhu, G., Basavaprabhu, Narendra, N., Vishwanatha, T. M., & Sureshbabu, V. V. (2015). Amino acid chlorides: A journey from instability and racemization toward broader utility in organic synthesis including peptides and their mimetics Dedicated to Professor Padmanabhan Balaram, Indian Institute of Science, Bangalore on the occasion of his superannuation. In *Tetrahedron* (Vol. 71, Issue 19, pp. 2785–2832). Elsevier Ltd. <https://doi.org/10.1016/j.tet.2015.03.026>
- Rastelli, A., Bagatti, M., & Gandolfi, R. (1995). Ab Initio Study of Concerted Cycloadditions of Allene, Monofluoroallene, and 1,1-Difluoroallene with Diazomethane, Formonitrile Oxide, Cyclopentadiene, and Furane. In *J. Am. Chem. SOC* (Vol. 117, Issue 1).
- Smith, G. G., & Sivakua, T. (1983). Mechanism of the Racemization of Amino Acids. Kinetics of Racemization of Arylglycines. *Journal of Organic Chemistry*, 48(5), 627–634. <https://doi.org/10.1021/jo00153a001>
- Smith, S. W. (2009). Chiral toxicology: It's the same thing only different. In *Toxicological Sciences* (Vol. 110, Issue 1, pp. 4–30). <https://doi.org/10.1093/toxsci/kfp097>
- Sturabotti, E., Vetica, F., Toscano, G., Calcaterra, A., Martinelli, A., Migneco, L. M., & Leonelli, F. (2023). N-Acetyl-L-phenylalanine Racemization during TBTU Amidation: An In-Depth Study for the Synthesis of Anti-Inflammatory 2-(N-Acetyl)-l-phenylalanyl-amido-2-deoxy-d-glucose (NAPA). *Molecules*, 28(2), 581. <https://doi.org/10.3390/molecules28020581>
- Takahashi, O., Kirikoshi, R., & Manabe, N. (2016). Racemization of the succinimide intermediate formed in proteins and peptides: A computational study of the mechanism catalyzed by dihydrogen phosphate ion. *International Journal of Molecular Sciences*, 17(10). <https://doi.org/10.3390/ijms17101698>
- Türker, L., Atalar, T., Gümüş, S., & Çamur, Y. (2009). A DFT study on nitrotriazines. *Journal of Hazardous Materials*, 167(1–3), 440–448. <https://doi.org/10.1016/j.jhazmat.2008.12.134>
- Yan, T., Feringa, B. L., & Barta, K. (2021). Direct Catalytic N-Alkylation of α -Amino Acid Esters and Amides Using Alcohols with High Retention of Stereochemistry. *ChemSusChem*, 14(11), 2303–2307. <https://doi.org/10.1002/cssc.202100373>
- Zeng, Y., Zhang, B., & Wang, M. (2017). Estimation of the racemization rate constants for α -amino acids using Density Functional Theory. *Computational and Theoretical Chemistry*, 1104, 43–46. <https://doi.org/10.1016/j.comptc.2017.01.034>

A. APPENDIX: METHODOLOGY CALCULATIONS

Table A-1: Main code lines for Gaussian 16 calculations.

Calculation	Main Codeline
Optimization + frequency for a reactant or intermediate.	<code># opt freq wb97xd/6-311++g(d,p) scrf=(smd,solvent=water)</code>
Optimization + frequency for a transition state.	<code># opt=(calcfc,ts,noeigentest) freq wb97xd/6-311++g(d,p) scrf=(smd,solvent=water)</code>
Intrinsic reaction coordinates	<code># irc=(forward,calcfc,maxpoints=1000,stepsize=1) wb97xd/6-311++g(d,p) nosymm pop=(always,minimal) scrf=(smd,solvent=water)</code>
Natural bond orbital	<code># irc=(forward,calcfc,maxpoints=1000,stepsize=1) wb97xd/6-311++g(d,p) nosymm pop=(always,mk,hirshfeld,minimal,nboread) polar output=wfn scrf=(smd,solvent=water)</code>

Table A-2: Thermal corrections of predicted thermodynamical results in gaseous phase to aqueous solution.

Parameter	Thermal Correction ¹
Enthalpy	$E_A^\ddagger = E'_A + 3RT$
Free energy	$\Delta H^\ddagger = \Delta H' + RT$
Activation energy ²	$\Delta G^\ddagger = \Delta G' - RT \ln R'T$

- E'_A , $\Delta H'$, and $\Delta G'$ are the predicted parameters in gaseous phase at a temperature of 383.45 K.
- R' is the gas constant with units L atm mol⁻¹ K⁻¹.

B. APPENDIX: CALCULATIONS RESULTS

Table B-1: Thermodynamic activation parameters of racemization, activation energy, enthalpy, Gibbs free energy and entropy at 383.45 K.

	X	Activation Energy ($kcal\ mol^{-1}$)		Enthalpy ($kcal\ mol^{-1}$)	Free Energy ($kcal\ mol^{-1}$)	Entropy ($cal\ mol^{-1}\ K^{-1}$)
		Smith & Sivakua	This work			
Aromatic	H	20.7	20.20	18.67	24.35	-14.80
	mCl	20.7	18.51	16.98	21.96	-12.97
	mNO ₂	20.8	17.25	15.72	21.58	-15.28
	pCl	20.3	19.19	17.66	23.82	-16.05
	pMe	21.1	20.98	19.46	25.55	-15.90
	pOMe	21.1	21.29	19.76	24.88	-13.36
Aliphatic	Leucine	27.9	27.27	26.57	33.10	-17.04
	Isoleucine	28.1	28.09	25.74	32.35	-16.43
	Phenylalanine	24.0	25.87	24.35	30.39	-15.75

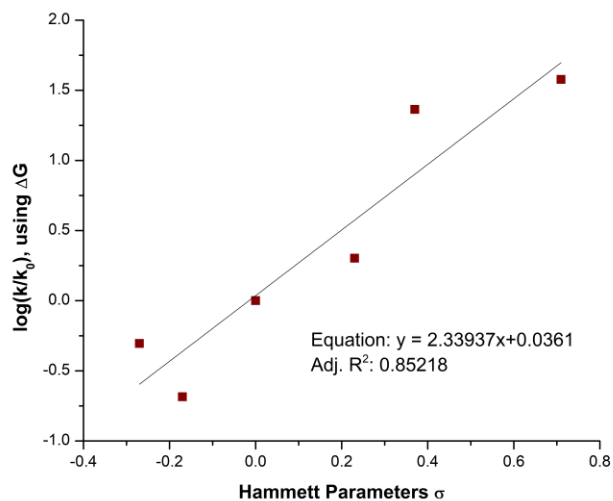


Figure B-1: Hammett σ plot using ΔG for calculations of kinetic constants.

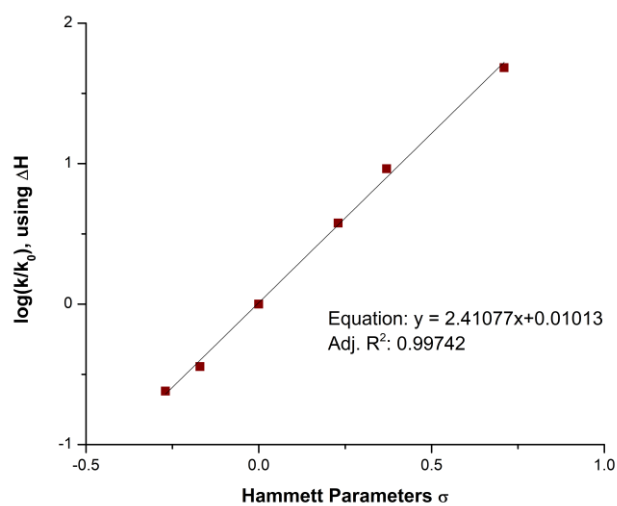


Figure B-2: Hammett σ plot using ΔH for calculations of kinetic constants.

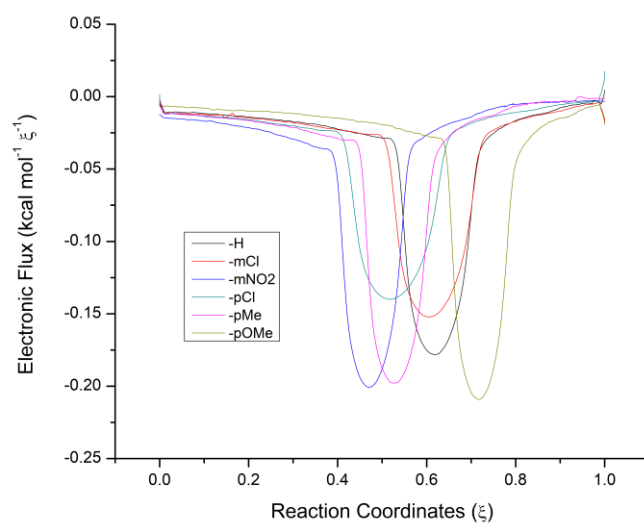


Figure B-3: IRC electronic flux profile for racemization of aromatic compounds.

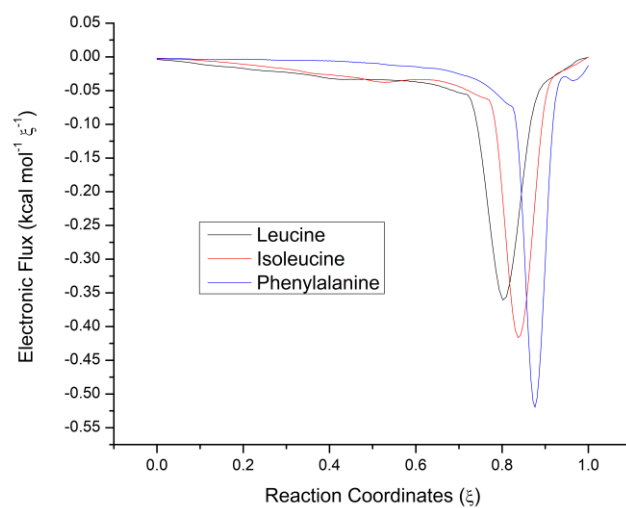


Figure B-4: IRC electronic flux profile for racemization of aliphatic compounds.

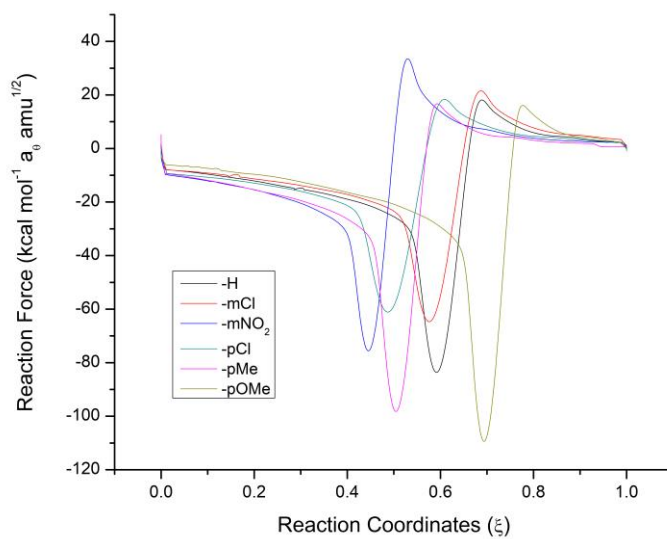


Figure B-5: IRC reaction force profile for racemization of aromatic compounds.

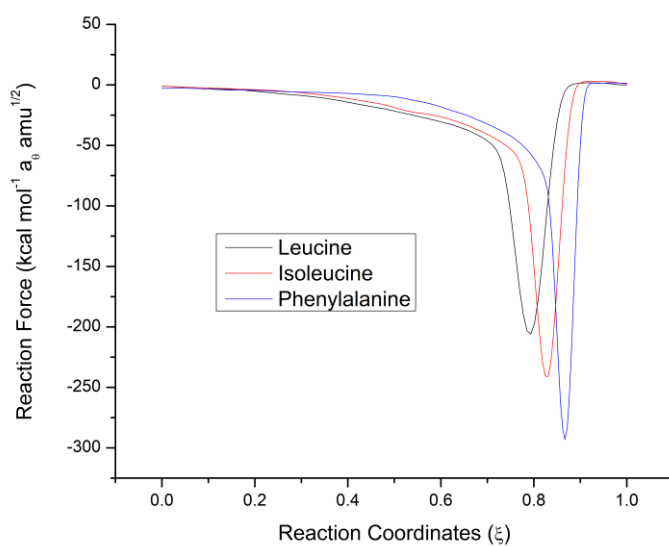


Figure B-6: IRC reaction force profile for racemization of aliphatic compounds.

Table B-2: Reaction works of H cleavage for racemization in kcal mol⁻¹.

	X	W ₁	W ₂	W ₃	W ₄	W ₁₄	W ₂₃
Aromatic	H	6.930775	2.972447	0.594285	4.379606	11.31038	3.566732
	mCl	5.420454	2.374458	0.860901	4.944634	10.36509	3.235359
	mNO ₂	4.969483	2.032308	1.050836	8.110897	13.08038	3.083144
	pCl	4.402541	2.401664	0.870441	6.01971	10.42225	3.272105
	pMe	6.778057	3.266344	0.514555	5.667308	12.44536	3.780899
	pOMe	9.274253	3.747533	0.389733	2.698293	11.97255	4.137266
Aliphatic	Leu	21.01251	7.479378	0.058778	0.069413	21.08192	7.538156
	IsoLeu	21.69717	6.686767	0.112253	0.133195	21.83036	6.79902
	PheAla	20.26074	6.445553	0.074244	0.048883	20.30963	6.519797

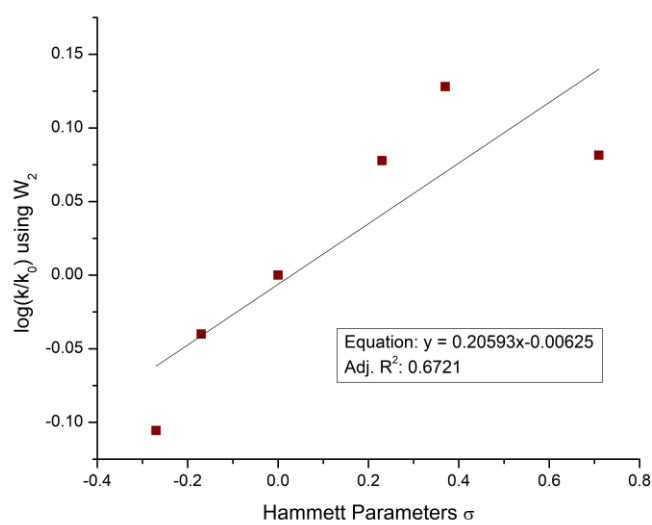


Figure B-7: Hammett σ plot using W_2 for calculations of kinetic constants.

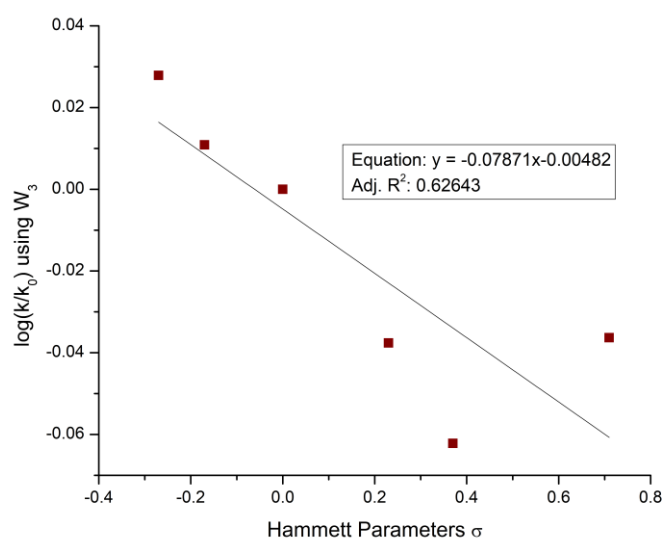


Figure B-8: Hammett σ plot using W_3 for calculations of kinetic constants.

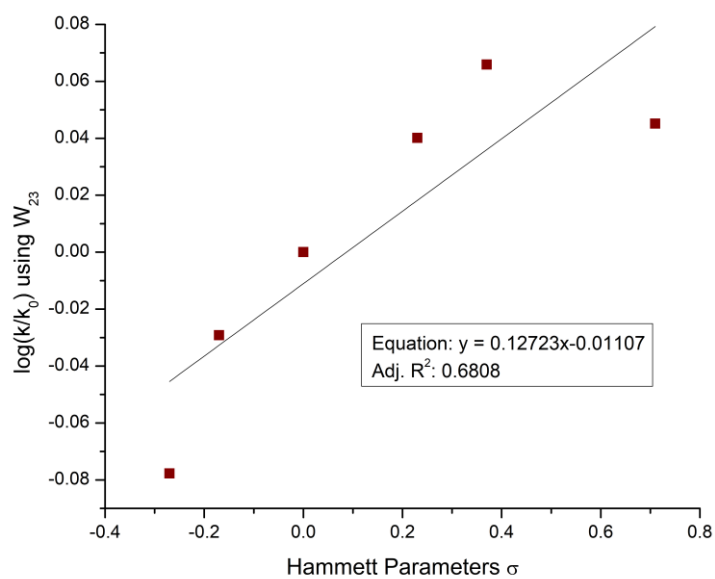


Figure B-9: Hammett σ plot using W_{23} for calculations of kinetic constants.

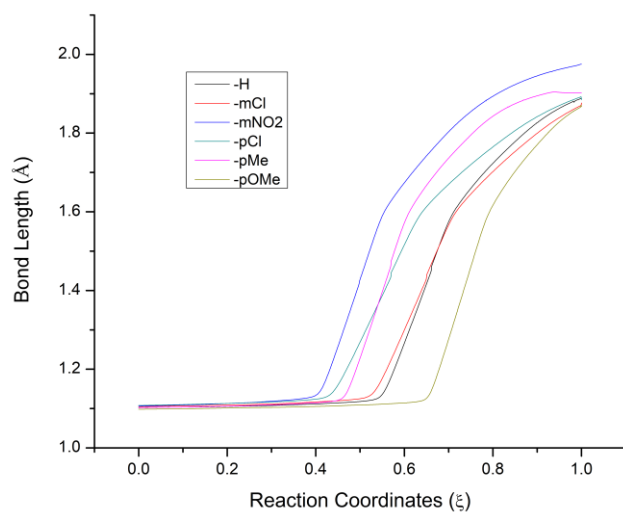


Figure B-10: IRC breaking of CH bond profile for racemization of aromatic compounds.

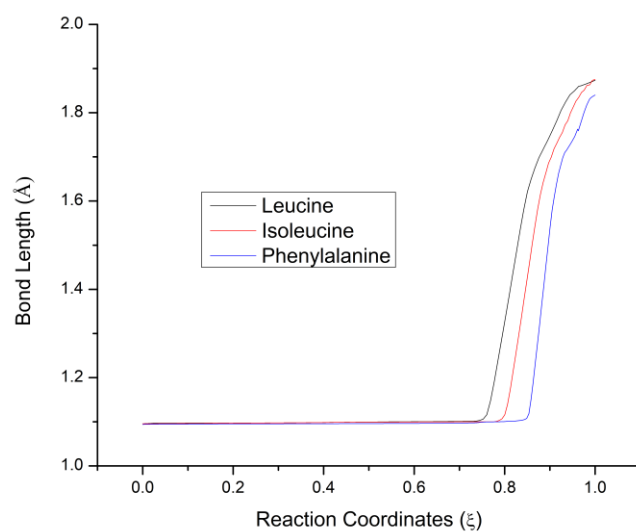


Figure B-11: IRC breaking of C1-H5 bond profile for racemization of aliphatic compounds.

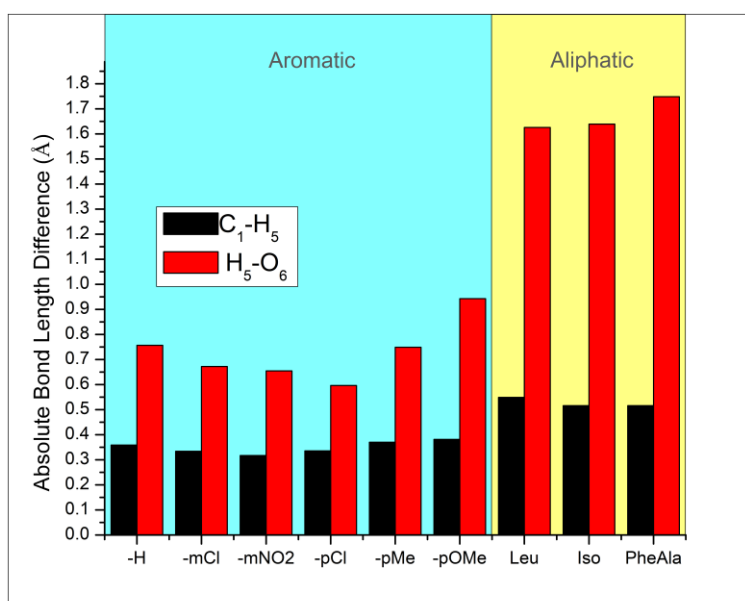


Figure B-12: Bond length difference from reactant to transition state. H5-O6 formation length diminishes and C1-H5 cleavage length increases.

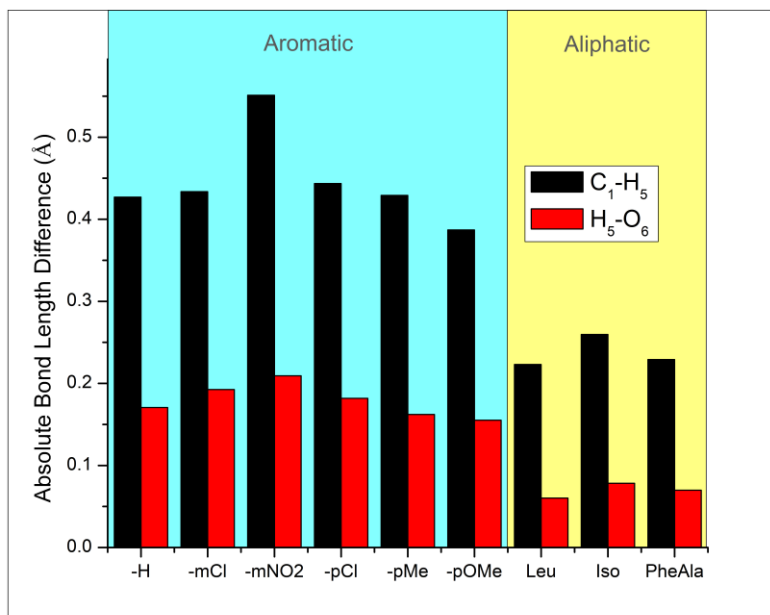


Figure B-13: Bond length difference from transition state to product. H₅-O₆ formation length diminishes and C₁-H₅ cleavage length increases.

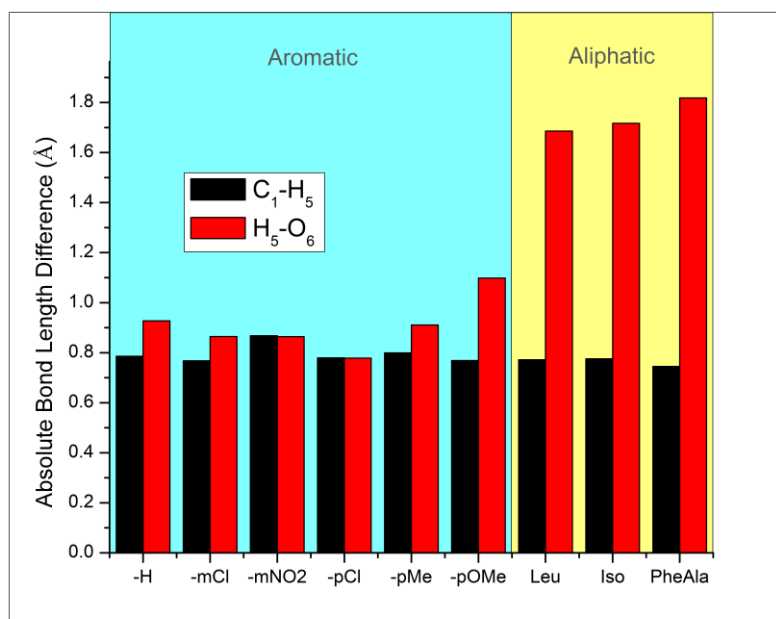


Figure B-14: Bond length difference from reactant to product. H₅-O₆ formation length diminishes and C₁-H₅ cleavage length increases.

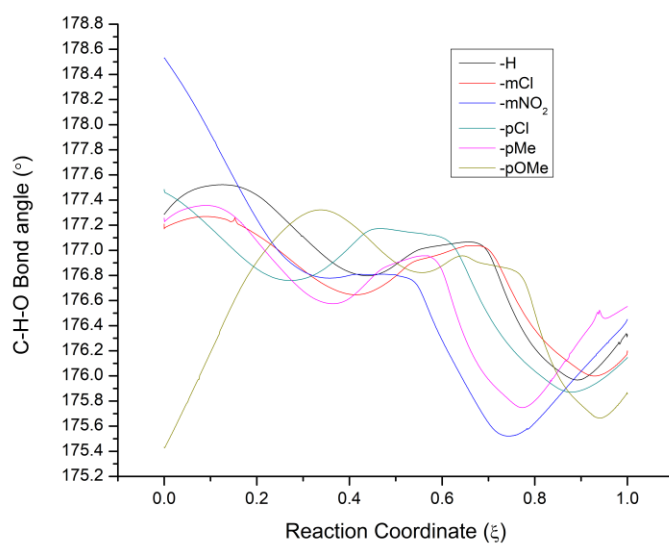


Figure B-15: IRC C1-H5-O6 bond angle profile for racemization of aromatic compounds.

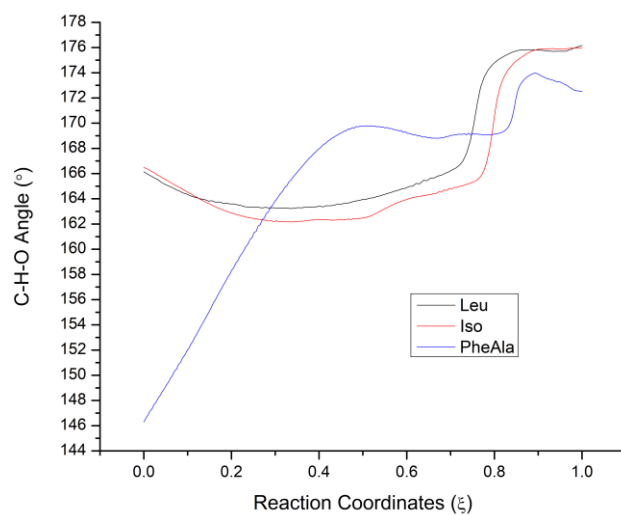


Figure B-16: IRC C1-H5-O6 bond angle profile for racemization of aliphatic compounds.

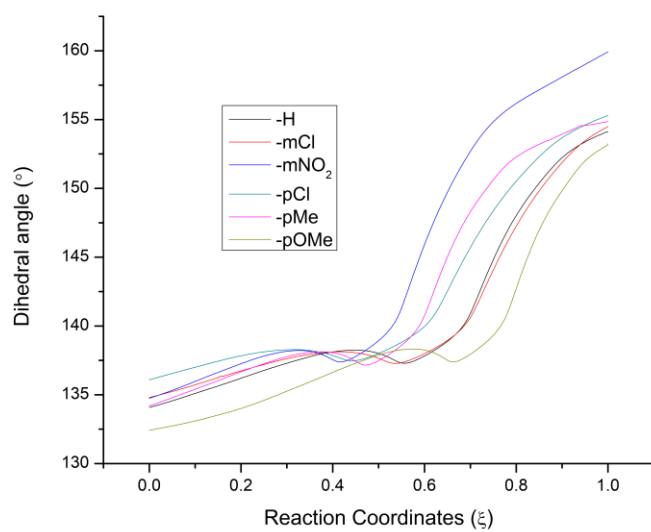


Figure B-17: IRC N3-C1-C2-C4 dihedral angle profile for racemization of aromatic compounds.

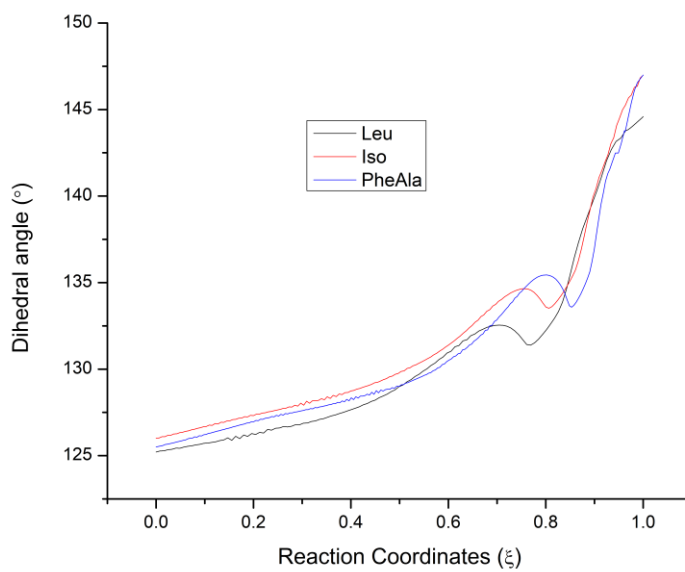


Figure B-18: IRC N3-C1-C2-C4 dihedral angle profile for racemization of aliphatic compounds.

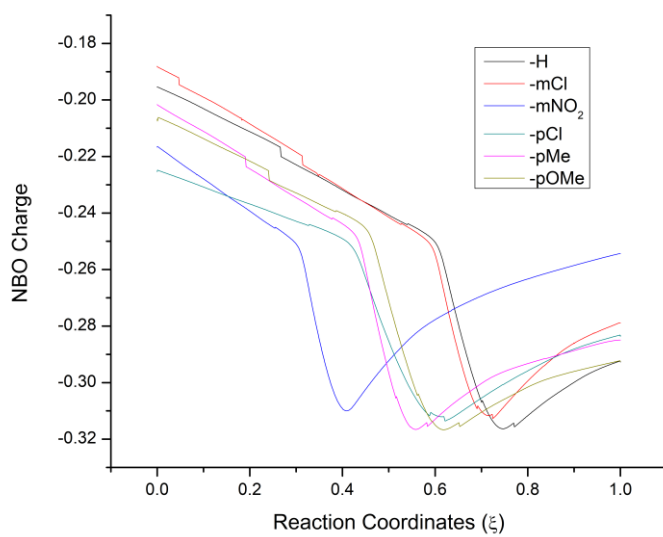


Figure B-19: Central carbon NBO charge profile for racemization of aromatic compounds.

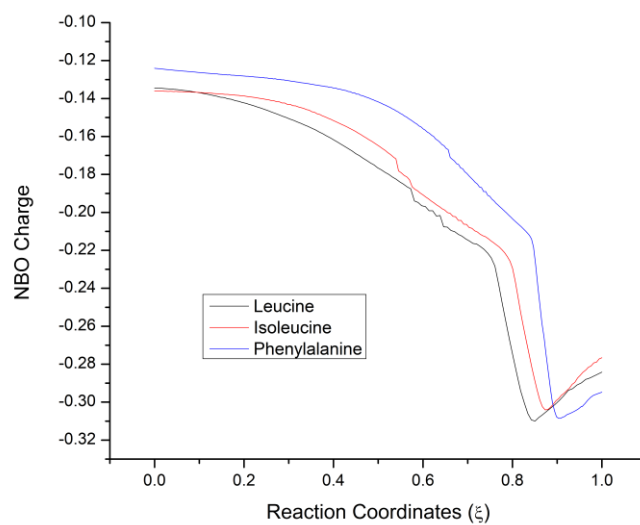


Figure B-20: Central carbon NBO charge profile for racemization of aliphatic compounds.

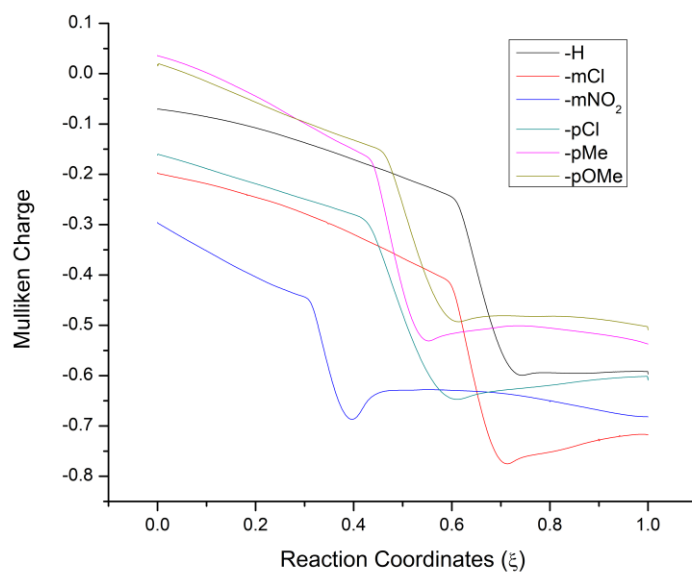


Figure B-21: Central carbon NBO charge profile for racemization of aliphatic compounds.

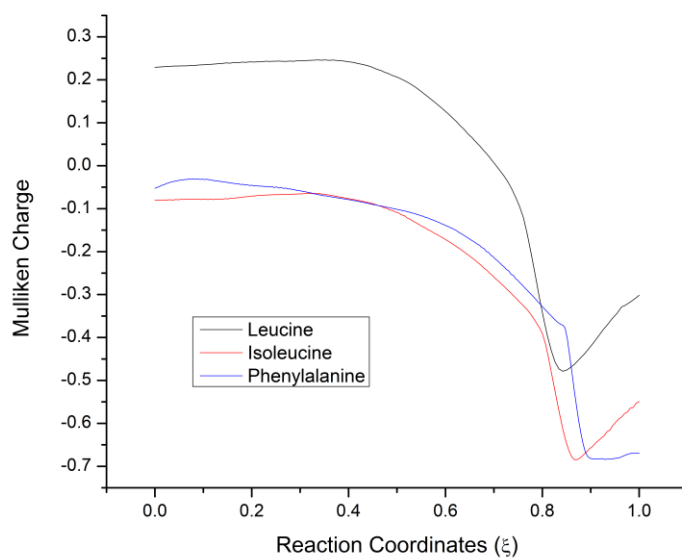


Figure B-22: Central carbon NBO charge profile for racemization of aliphatic compounds.

Table B-3: Square correlation coefficient R^2 and slope m of linear regression between NBO charges of reactant (R), transition state (TS), and intermediate (I) and experimental energy of activation.

Atom		R	TS	I	TS-R	I-TS	I-R
C ₁	R ²	0.757 ²	0.178	0.013	0.721	< 0.001	0.602
	m	0.0110 ³	0.0004	0.0004	-0.0106	> -0.0001	-0.0107
C ₂	R ²	0.026	0.906	0.982	0.951	< 0.001	0.983
	m	0.0002	-0.0078	-0.0078	-0.0080	> -0.0001	-0.0080
N ₃	R ²	0.948	0.988	0.989	0.933	0.827	0.552
	m	-0.0025	-0.0039	-0.0032	-0.0014	0.0007	-0.0007
C ₄	R ²	0.675	0.676	0.673	0.372	0.571	0.023
	m	-0.0434	-0.0446	-0.0431	-0.0012	0.0015	0.0003
H ₅	R ²	0.865	0.907	0.385	0.454	0.833	0.184
	m	-0.0135	0.0044	-0.0008	0.0109	-0.0052	0.0058
O ₆	R ²	0.753	0.804	0.759	0.701	0.799	0.014
	m	-0.0052	0.0064	-0.0032	0.0089	-0.0096	-0.0007

2. The highest correlation for each atom is highlighted in blue.
3. The highest absolute slope value for each atom is highlighted in purple.

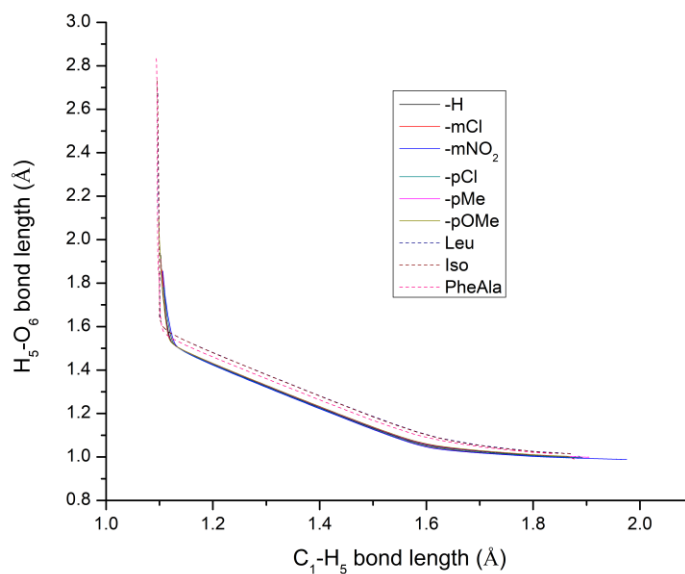


Figure B-23: Bond length comparison between the C1-H5 bond and H5-O6 across IRC calculations.

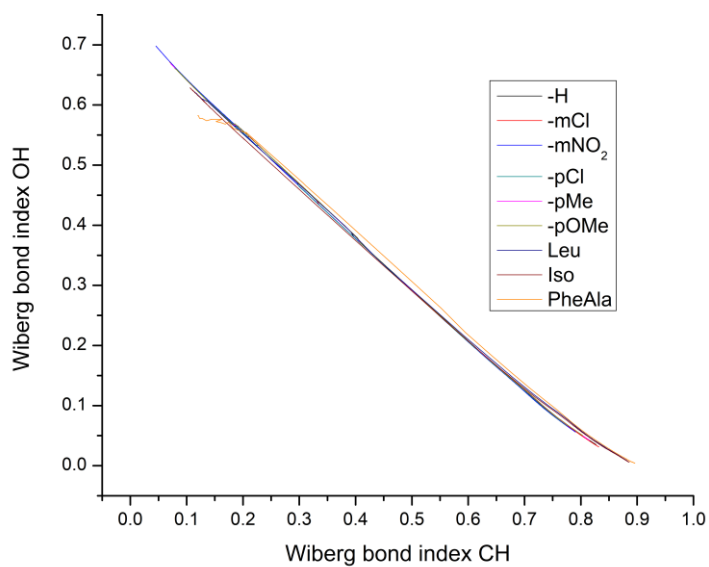


Figure B-24: Wiberg bond index comparison between the C1-H5 bond and H5-O6 across IRC calculations.

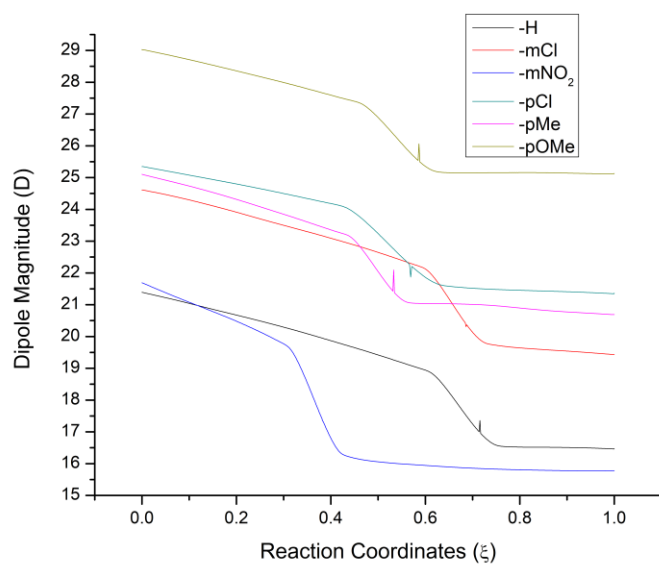


Figure B-25: IRC dipole profile for racemization of aromatic compounds.

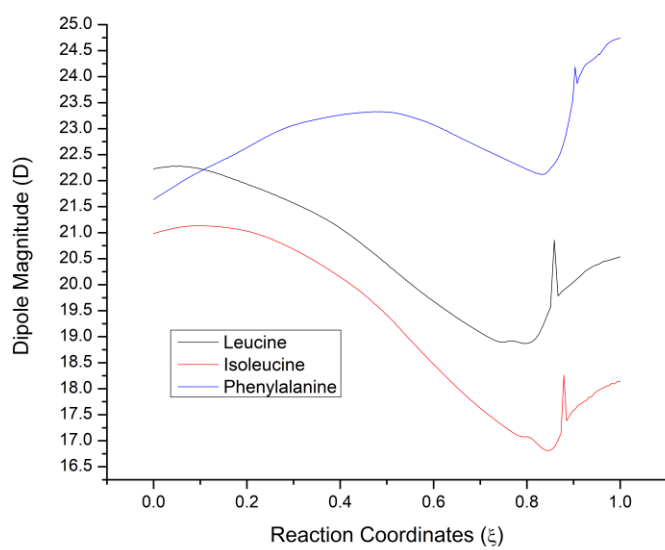


Figure B-26: IRC dipole profile for racemization of aliphatic compounds.

C. APPENDIX: MISCELLANEOUS

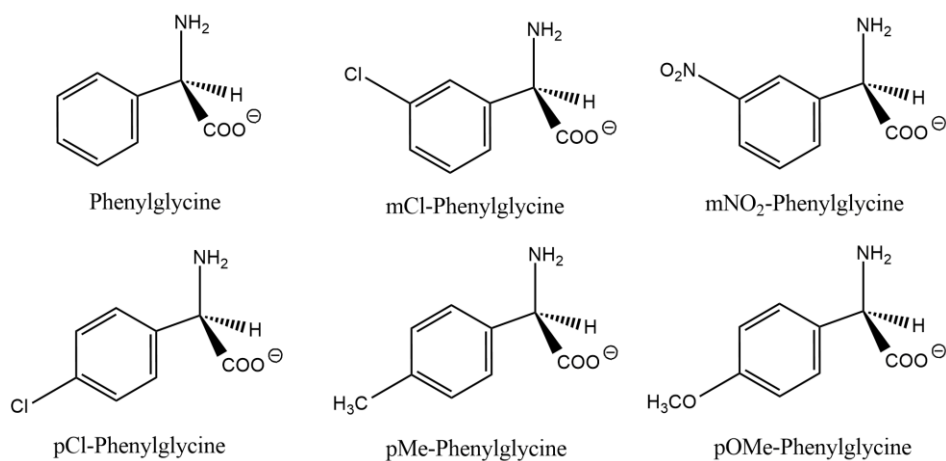


Figure C-1: Aromatic amino acids.

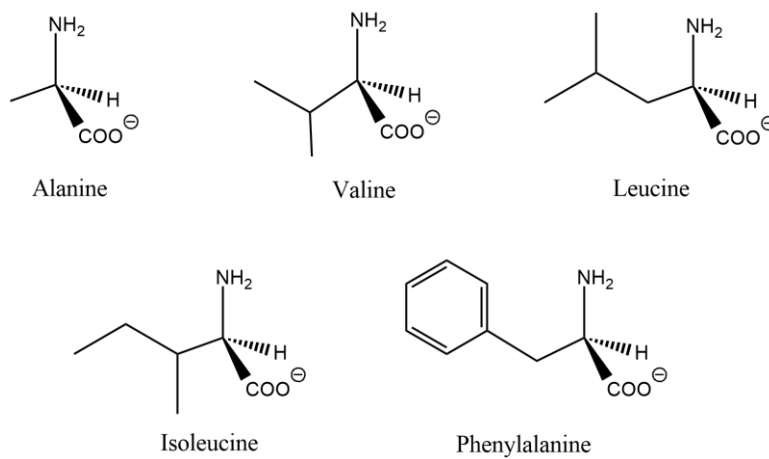


Figure C-2: Aliphatic amino acids.

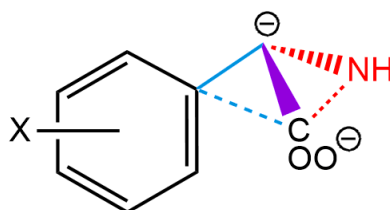


Figure C-3: N3-C2-C1 (red) and C2-C1-C4 (blue) planes considered in dihedral angle calculations.